Tuijin Jishu/Journal of Propulsion Technology
ISSN: 1001-4055
Vol. 46 No. 1 (2025)

Geothite as Propellant Grade Catalyst – Preparation and Characterisation

O. Sai Siddhartha[1], S.V. Satyanarayana[2]

[1]*Research Scholar, Jawaharlal Nehru Technological University Anantapur, Ananthapuramu*
[2]*Director of Evaluation, JNTU Anantapur, Ananthapuramu, Andhra Pradesh, India*

Abstract:

The increasing demand for higher acceleration during the first 100 seconds of rocket ascent drives rocket propellant designers to explore advanced materials. One key area of focus is the development of combustion catalysts for composite solid propellants. While iron oxide is a commonly used catalyst in solid propellants globally, detailed data is scarce because its formulation is often tailored to specific fuel-oxidizer compositions. This paper aims to develop high surface area propellant-grade iron oxides with a modified version of the David and Welch method. Our approach is twofold: first, we alter the process conditions of the David and Welch method and prepare high surface area propellant-grade iron oxides; second, we extensively characterised the prepared catalyst and conducted propellant level trials. Lowering the process temperature and using hot air oven in one experiment and open-air drying in another resulted in the formation of iron oxyhydroxide structures. Structural analysis was performed using X-ray diffraction (XRD) supplemented by Mossbauer, FTIR, EDS, and Raman spectroscopies. The surface morphology was examined using field emission scanning electron microscopy (FESEM), and specific surface area was measured using the BET method where higher surface area of approximately 100 m^2/g was achieved. Iron oxy hydroxide particles were needle-like, non-agglomerated and amorphous in nature. The propellant viscosity and viscosity build-up rate showed no abnormalities, indicating no adverse effects on rocket castability and pot life. Similarly, the uniaxial mechanical properties (tensile strength, elongation at break, Young's modulus, and hardness) were within acceptable limits for existing propellants. However, the iron oxyhydroxide prepared using open-air drying exhibited low viscosity build-up, reduced Young's modulus, and hardness, likely due to surface moisture reducing the presence of curative in the polymer network. Burn rate measurements were conducted using acoustic emission (AEBR) and ultrasonic emission (UBR) techniques, which also assessed burn rate sensitivity and pressure index. The results indicate that both the samples enhanced burn rate and pressure index compared to a catalyst-free sample.

Keywords*: Composite Solid Propellants, Iron Oxide Synthesis, Acoustic Emission Burn Rate (AEBR), Ultrasonic Burn Rate (UBR)*

1. Introduction

Space begins at an altitude of 100 km, where Earth's atmosphere no longer exists as it does at the surface. This region is vital for satellite deployment and Earth observation. Rockets, requiring velocities around 1.4 km/s to reach this zone, are powered by propellants that combust rapidly to achieve high thrust. Solid propellants, widely used in rocketry, offer simplicity, reliability, and cost-effectiveness. These consist of a fuel-oxidizer mixture bound in a solid state, burning at controlled rates to generate thrust. Catalysts, like Copper Chromite and Ferric Oxide enhance burn rates and combustion efficiency without necessitating thicker rocket chambers. Composite solid propellants typically include ammonium perchlorate (oxidizer), aluminum powder (fuel), and hydroxyl-terminated polybutadiene (binder/fuel). Additives like burn rate modifiers and stabilizers fine-tune performance. The typical formulation is given in Table 1. Copper Chromite, leveraging dual electron donor/acceptor mechanisms, and Ferric Oxide, with Lewis acidic sites, are key combustion catalysts in modern formulations, improving burn rates and propellant stability. This work focuses on developing an iron oxide-based catalyst optimized for HTPB/AP/Al propellants, balancing performance and safety in space exploration [1-3].

Table 1: Typical Composite Solid Propellant Formulation [1]

Component	Purpose	Typical Percentage (%)
Ammonium Perchlorate (AP)	Oxidizer	60-70%
Aluminum Powder (Al)	Fuel	15-20%
Hydroxyl-terminated polybutadiene (HTPB)	Binder/Fuel	10-15%
Plasticizers	Enhance flexibility and processability	1-5%
Stabilizers	Prevent decomposition	0.5-2%
Burn Rate Modifiers	Control burn rate and enhance decomposition	0-0.5%
Curing Agents	Cross-linking agents for binder	0.5-1%

The mutual ratio of these components depends on a trade-off between the expected heat of combustion and the efficiency of converting this thermal energy into the kinetic energy of product gases, defined as specific impulse. While the heat of combustion does not depend on the catalyst, the efficiency of energy conversion is mildly influenced by changes in the molecular weight of the products. In summary, catalysts can enhance the burn rate and efficiency of propellants without the drawbacks associated with increasing pressure, such as the need for a thicker and heavier rocket chamber. This makes them an essential component in modern rocket propellant formulations, ensuring optimal performance in space travel where carrying oxidizers and efficiently converting chemical energy into thrust are vital [4].

2. Experimental Work

In this study, we modified the process parameters, including temperature, stirrer RPM, and drying methodology, based on the David and Welch method [5]. This conventional laboratory preparation technique begins with ferrous sulphate, which undergoes nitration using potassium nitrate (KNO_3), followed by hydroxylation with potassium hydroxide (KOH). The resulting precipitate is then thoroughly washed and dried in a vacuum oven for an extended period. The method is highly sensitive, with even minor variations in any step potentially resulting in the formation of different ferric oxide phases. Furthermore, the type of intermediate formed during the process plays a critical role in determining the characteristics of the final product. In this work, we specifically investigated:

a) The impact of reducing the process temperature.
b) The influence of altering the drying temperature.

2.1. Materials for catalyst preparation

The materials used for preparing the catalyst are $FeSO_4.7H_2O$ (98%, MERCK), KNO_3 (98%, MERCK), KOH (98%, MERCK), DM Water (In-house prepared), Filter Paper

2.2. Equipment

Laboratory Glassware, Peristaltic Pump, Overhead Stirrer, Vacuum Oven, Hot Air Oven, Grinder, pH meter

2.3. Catalyst Preparation Method

The experimental procedure has the following steps:

a. 400 g of $FeSO_4.7H_2O$ was dissolved in 2240 ml of DM water in a flask at room temperature.
b. 224.5g of KOH and 32.3g of KNO_3 were mixed in 1200 ml of DM water in another flask at room temperature.
c. Add the ferrous sulphate solution to a flask with an overhead stirrer arrangement and keep the stirrer at 15000 rpm for effective dispersion and homogenization.
d. Subsequently, the mixture of potassium hydroxide and potassium nitrate solutions were added drop wise to this flask at room temperature for two hours. This addition was meticulously controlled using a peristaltic pump to ensure precise delivery and uniform mixing.
e. After completion of addition, the solutions were stirred for another 30 minutes at 15000 rpm at room

temperature.

f. Then the solution with precipitate was allowed to cool and settle overnight.

g. The precipitate with pH around 12-14, was washed with DM water several times until the pH of the wash liquid was around 7. Industrial grade filter paper was used to separate the wash liquid and precipitate.

h. The wet cake collected on the filter paper was divided into two batches. One batch was dried in a hot air oven at 110^0C for 8 hours and another batch was left to dry in a tray for 5 days at room temperature.

i. The dried material was in the form of agglomerates and thus was ground using a domestic grinder.

j. Fig-1 shows the typical sketch of the experimental setup.

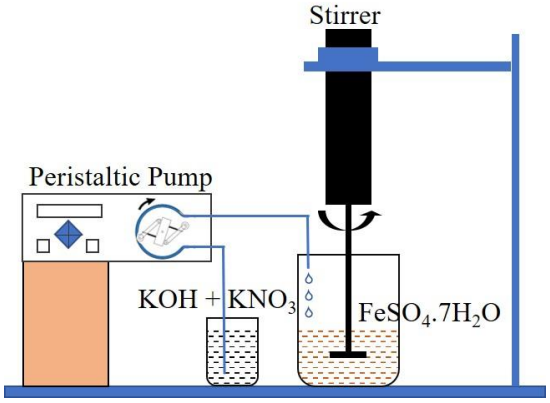

Fig. 1 Catalyst Preparation Setup

k. The material dried in hot air oven is designated as IO-2 and the material dried in open atmosphere is designated as IO-3.

2.4. Propellant Preparation Method

Typical steps followed in the propellant preparation are outlined in figure 2 below

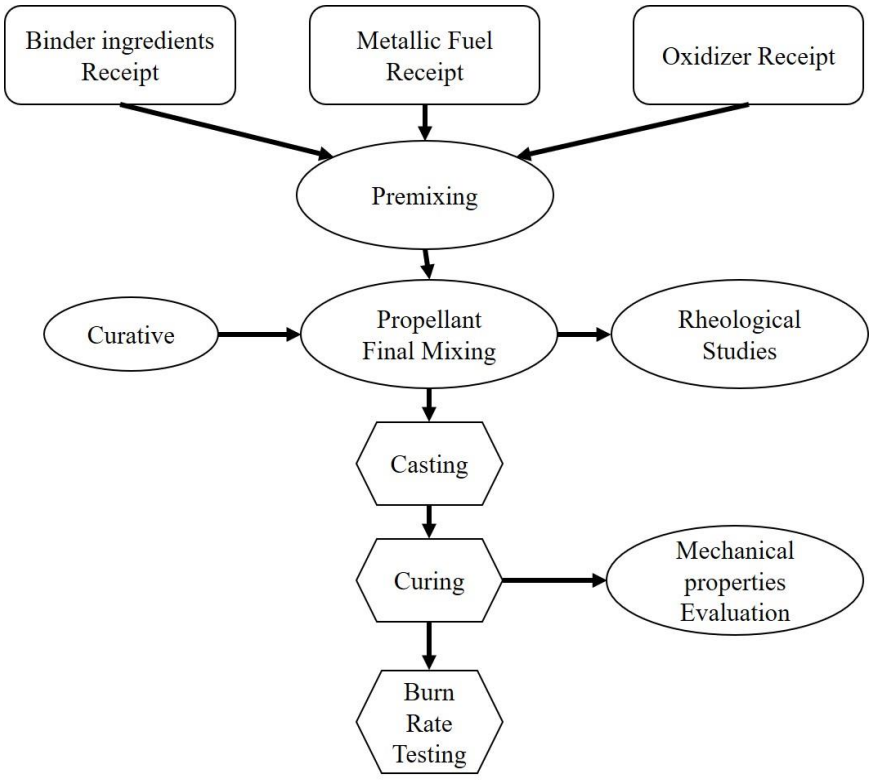

Fig. 2 Process Flow Diagram for Propellant Slurry Preparation & Characterisation

2.5. Catalyst Characterisation

The following analysis was carried out to understand the catalyst properties:

a. Average Particle Size – The Fisher Sub-Sieve Sizer is used for the measurement of average particle size. It operates on the air-permeability principle. The air pump builds up air pressure to a constant head in the pressure regulated standpipe. Under this pressure head, air passes through the packed powder sample contained in the sample tube. The flow of air through this packed bed is measured by means of a calibrated manometer; in which the level of the fluid indicates the average diameter of the powder directly on the calculated chart.

b. Surface area by BET method - Brunauer-Emmett-Teller (BET) surface area is estimated by nitrogen adsorption-desorption isotherm measurements on Quantachrome NOVA 4000e equipment.

c. XRD - X-ray diffraction (XRD) was employed to investigate the crystalline structure, phase composition, and microstructural properties of the synthesized material. We used PANalytical (Empyrean) X-ray diffractometer with Cu Kα source operated at 40kV, 30 mA, and the diffraction data are recorded in the 2θ range of 10°-80° with a standard monochromator provided with a Ni filter to avoid Cu Kβ interference.

d. FTIR - FTIR spectrum was taken using Thermo scientific Nicolet iS50 FTIR spectrometer. A transmission infrared spectrum is a plot of percent radiation absorbed versus the frequency of the incident radiation given in wavenumbers (cm^{-1}). Increased resolution is provided by Fourier Transform IR (FTIR) which averages a large number of spectra and gives an improved signal to noise ratio and hence increased sensitivity compared with conventional IR spectroscopy. FTIR also permits more rapid collection of data.

e. FESEM-EDS - The morphology of the material was studied by field emission scanning electron microscopy (FESEM) on a JOEL JSM-7610F equipped with an Oxford Instruments energy dispersive spectroscopy (EDS) analyser for the elemental analysis.

f. Raman Analysis – Raman measurements of samples were carried out using WITec alpha 300R Confocal Raman Microscope. Five spectra were accumulated with an integration time of 5 seconds to obtain an average Raman spectrum. Raman spectrum was recorded with laser source of 532 nm (UV-Vis region) excitation.

g. Mossbauer Spectroscopy - Among the spectroscopic methods, Mossbauer spectroscopy (nuclear resonant γ-ray absorption spectroscopy) has the great advantage of being element-specific and as ^{57}Fe is a convenient Mossbauer active isotope, the technique is suitable for iron oxides. It supplies information about the magnetic field at the nucleus, the valence of the Fe and the type of coordination and order within the ligand shell.

h. Propellant Characterization

Propellant is prepared incorporating the iron oxides so prepared and test fired. The propellant is characterized as follows:

1. Viscosity measurement for the uncured propellant samples was done using Brookfield Viscometer with a helipath stand at a process temperature of 40^0C (Fig. 3) at a strain rate of 2 rpm of a selected spindle.
2. The mechanical properties of cured samples were evaluated using dumbbells punched out from 5 mm thick propellant slabs as per ASTM D-412 type-C at a cross head speed (strain rate) of 50 mm/min at 25^0C (Fig. 4). The specimens for mechanical properties are thermally soaked at 25^0C, 30-50% RH for a minimum of 24 hours prior to testing. The modulus is measured at 3% of strain in order to get the modulus at elastic region as a standard procedure which depends on the propellant formulation.
3. The burn rate of the cured propellant samples was evaluated by two independent methods viz., acoustic emission (AE) technique and Ultrasonic burn rate (UBR) technique at a pressure of 40 ksc. AE technique is employed in the area where new propellant formulations are being developed due to limited quantity of propellant available during developmental phase. In general, UBR is used to provide burn rate values of propellants to find out augmentation factor to predict actual motor performances.

a) Measurement of burning rate of solid propellant using AE method employs the capture and amplification of sound/ acoustic signal generated during the underwater burning of the specified length of solid propellant strand (6 mm x 6 mm x 90 mm). In this method the burning time is computed based on time difference between the initial and final peak of the amplified acoustic signal. Subsequently, the burning rate is evaluated from the length and time difference computed from the acoustic emission signal (Fig. 5).

b) In Ultrasonic burn rate technique, solid propellant burn rate is measured based on the velocity of the propagated sound wave through the propellant sample of size Φ35 mm x L 40 mm. Time of burning is computed

based on the difference between transmitted and received sound signal at each instance of burning. Subsequently length burnt during the process is computed based on the calibrated sound velocity through the medium (Fig. 5).

c) The temperature coefficient (a) and burn rate index (n) are evaluated by nonlinear regression of the variation of burning rate with pressure. The relation among pressure and burn rate of solid propellant is expressed by Saint Robert's law [6] as:

$$R = a.P^n \rightarrow (1)$$

R = Burning rate of solid propellant, $mm.s^{-1}$

a = Burning rate temperature coefficient, $mm.\ s^{-1}.\ mPa^{-n}$

P = Chamber pressure, mP_a

n = Burn rate index

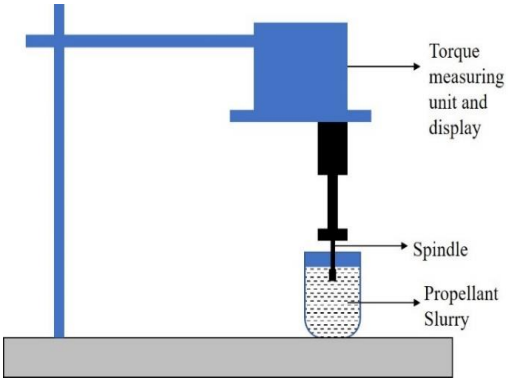

Fig. 3 Brookfield Viscometer Setup

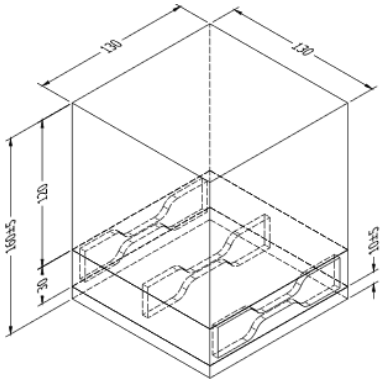

Fig. 4a. Dumbbell Punching Methodology

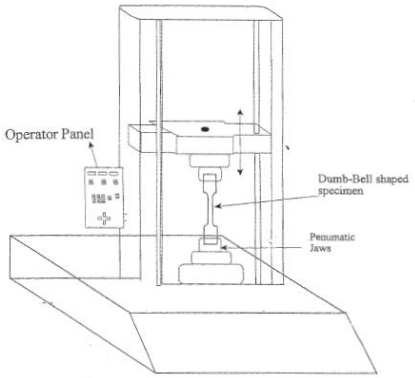

Fig. 4b. Universal Testing Machine

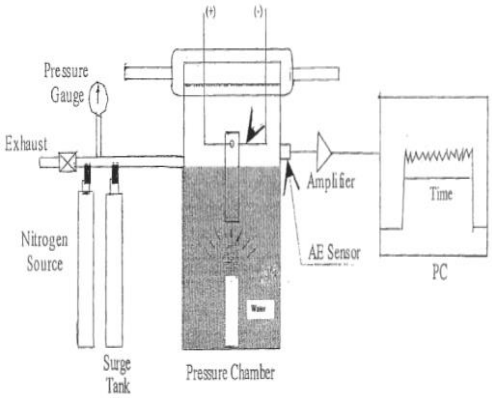

Fig. 5a Schematic Sketch of AE Burn Rate Measuring Setup

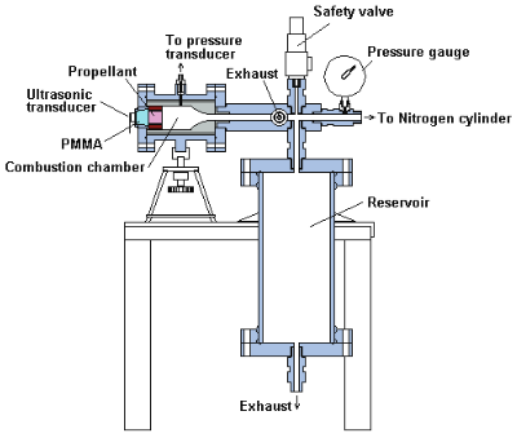

Fig. 5b UBR Test Setup

3. Results & Discussion

This section is structured into two parts. The first part presents the experimental results following characterization, the second part illustrates the results of the propellant experiments and provides discussion on these results.

3.1. Results of Experiments and Catalyst Characterization

A. Experiment-1, IO-2:

a) Physical Properties

Table-2: Estimated Physical properties of IO-2

S.No.	Property	Result
1.	Density	3.62 g/cc
2.	Average Particle Size	1.55 µ
3.	Magnetism	Non-magnetic

b) Particle characterization

The results of specific surface area (SSA) and SEM are given below.

i. SSA: The BET Surface area obtained is 107 m^2/g. This is a very large value. There are two possibilities which can explain this value. One, assuming no much agglomeration, all the particles are exposed to N_2 adsorption leading to high SSA. On the other hand, even if agglomerates present, they may have porosity to the extent of N_2 adsorption.

ii. SEM: SEM photo plates at various resolutions ranging from 25000X to 200000X are given in Fig. 6. From the SEM Images, two points are inferred, a) the particles are rod like, to the extent of calling them fibrous and b) the images are found hazy or blurred, due to a possible beam shift, and is attributed to large volatile matter (0.9%). The morphology and the presence of -OOH suggest goethite as the structure. The high surface area is justified from the SEM. SEM also indicated a very low degree of agglomeration and random packing of the particles leading to voids or porosity. This void fraction perhaps is the reason for entrapment of surface moisture/ volatile matter.

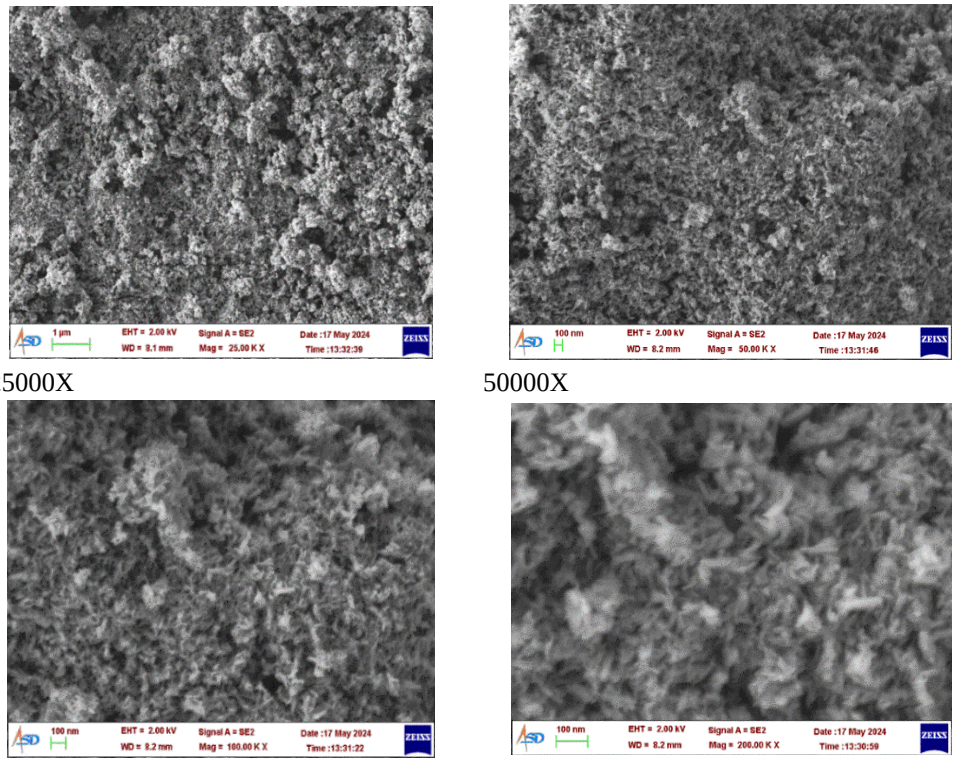

Fig. 6: SEM photo plates of IO-2 with different magnifications

c) Crystallography

1. XRD spectrum: The spectrum is shown in Fig. 7 and the corresponding peak positions including the derived particle size are presented in the Table 3. The particle size is from 8-16 nm although a few existed at 142 nm. The analysis indicates that these peaks align with the database entries for α-FeOOH as shown in Table 4. Table 5 illustrates the corresponding crystal dimensions.

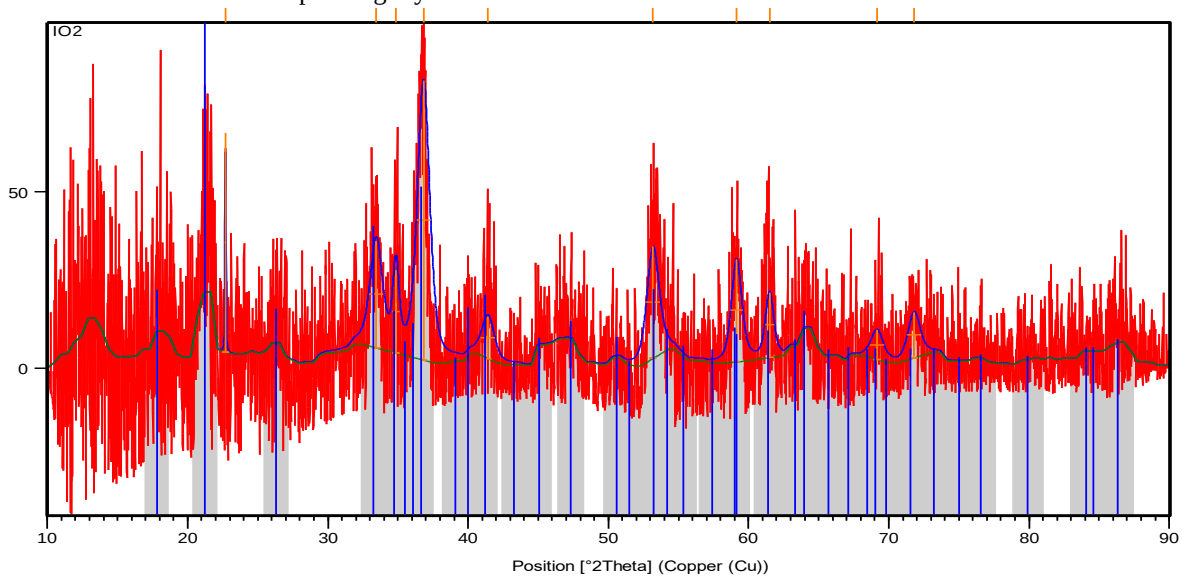

Fig. 7: XRD spectrum of IO-2

Table-3: Peak List of IO-2

Pos. [°2Th.]	Height [cts]	FWHM Left [°2Th.]	d-spacing [Å]	Rel. Int. [%]	Size, nm
22.7008	62.00	0.0648	3.91395	78.36	142.2
33.4503	30.32	1.0368	2.67669	38.33	8.1
34.8579	23.57	0.5184	2.57175	29.79	16.3
36.8270	79.12	1.0368	2.43864	100.00	8.1
41.4298	11.93	1.0368	2.17772	15.08	8.3
53.1958	31.67	1.0368	1.72047	40.03	8.6
59.1538	29.07	0.8640	1.56060	36.74	10.7
61.5039	18.36	0.6912	1.50648	23.20	13.5
69.1743	8.41	1.0368	1.35697	10.63	9.4
71.8078	13.02	1.0368	1.31355	16.45	9.5

Table-4: Composition of IO-2 as derived from XRD

Reference Code	Compound Name	Chemical Formula	No. of formula units per unit cell	Calculated density
01-081-0464	Goethite	FeO(OH)	4	4.26 g/cm^3

Table-5: Crystal dimensions of the components of IO-2 as derived from XRD

Compound Name	Crystal System	Space group	a, Å	b, Å	c, Å	α	β	γ
Goethite	Orthorhombic	Pbnm	4.6048	9.9595	3.0230	90^0	90^0	90^0

2. EDS Spectrum: The EDS spectrum is shown in Fig. 8. EDS data suggests 58.87% of Fe and 41.13% O_2, which is close to goethite. It is on par with the XRD analysis, discounting on occluded moisture affecting the exact percentages.

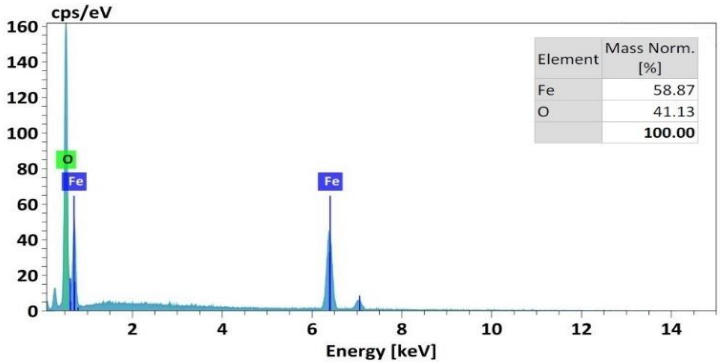

Fig. 8: EDS spectrum of IO-2

3. FTIR Spectrum: The FTIR spectrum of IO-2 is given in Fig. 9. The peaks are observed at 3128, 889, 793, 622 cm^{-1}. 3128 cm^{-1} is often associated with the O-H stretching vibration of hydroxyl groups (OH) in goethite. 889 cm^{-1} corresponds to the Fe-O stretching vibration in iron oxides, particularly characteristic of goethite. 793 cm^{-1} is typically attributed to the Fe-O bending vibration in iron oxides, which is also seen in goethite. Peak at 622 cm^{-1} is assigned to the O-H bending vibration, another characteristic feature of goethite. Therefore, based on the FTIR peaks provided, the material is likely goethite (α-FeOOH).

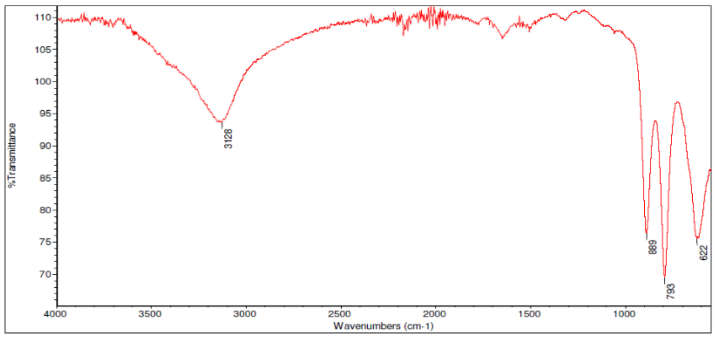

Fig. 9: FTIR Spectrum of IO-2

4. Raman Spectrum: Fig. 10 is the Raman spectrum signature. Peak at 216 cm^{-1} is attributed to the bending mode of the Fe-O-H group in goethite. It is a key feature for identifying goethite, as this peak is relatively distinctive for this iron oxide hydroxide mineral. Peak at 282 cm^{-1} is associated with the stretching vibrations of the Fe-O bonds within the goethite structure. This mode further supports the identification by confirming the presence of goethite's characteristic iron-oxygen bonding.

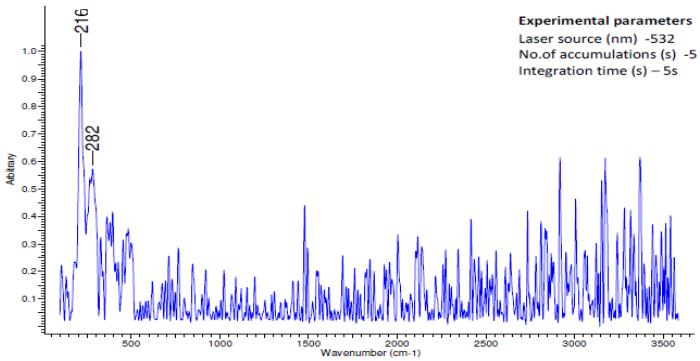

Fig. 10: Raman spectra of IO-2

5. Mossbauer Spectrum: The Mossbauer spectrum of IO-2 is shown in Fig. 11. The interpreted data is given in Table-6. From the table and spectrum, it is understood that the BHF value of <25.9> Tesla is lower than typical values for goethite, but could suggest a super paramagnetic state or smaller particle size. The absence of provided ISO and QUA makes it challenging to conclusively identify goethite, but the low BHF raises the possibility of a less magnetically ordered phase, like goethite.

Table-6: Mossbauer Spectrum Parameters of IO-2

IO-2	Width (mm/s)	ISO (mm/s)	QUA (mm/s)	BHF (Tesla)	% Area
Component 1	0.45	-	-	<25.9>	100

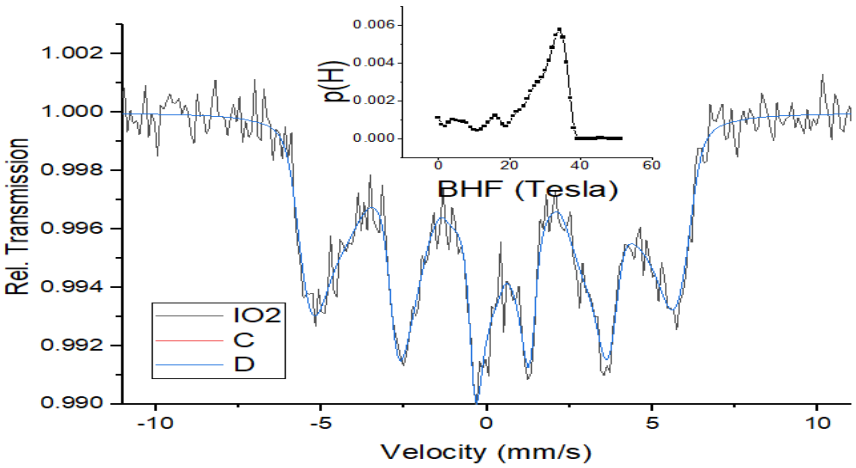

Fig. 11: Mossbauer Spectrum of IO-2

In summary, IO-2, prepared using the basic David and Welch method, bringing the process temperature to room temperature and drying to 110^0C exposing to air resulted in the formation of non-magnetic goethite (α-FeOOH) elongated rod-like/ fibrous/ needle-like particles without much agglomeration leading to very high surface area. The particles are randomly packed leading to visible porosity or void fraction where the volatile matter (surface moisture) is entrapped.

B. Experiment-3, IO-3

a) Physical Properties

Table-7: Estimated Physical properties of IO-3

S.No.	Property	Result
1.	Density	3.03 g/cc
2.	Average Particle Size	3.00 µ
3.	Magnetism	Non-magnetic

b) Particle characterization

i. SSA: The BET Surface area obtained is 99.7 m^2/g. This value is in line with IO-2.

ii. SEM: SEM photo plates at various resolutions ranging from 25000X to 200000X are given in Fig. 12. Again, like IO-2, SEM Images appeared blurred due to surface moisture. The SEM images suggests that a) the particles are elongated rod-like/ fibrous/ needle-like particles b) the degree of agglomeration is less and c) the particles are randomly packed leading to high void fraction even more than the IO-2 sample. This void fraction perhaps is the reason for entrapment of surface moisture/ volatile matter.

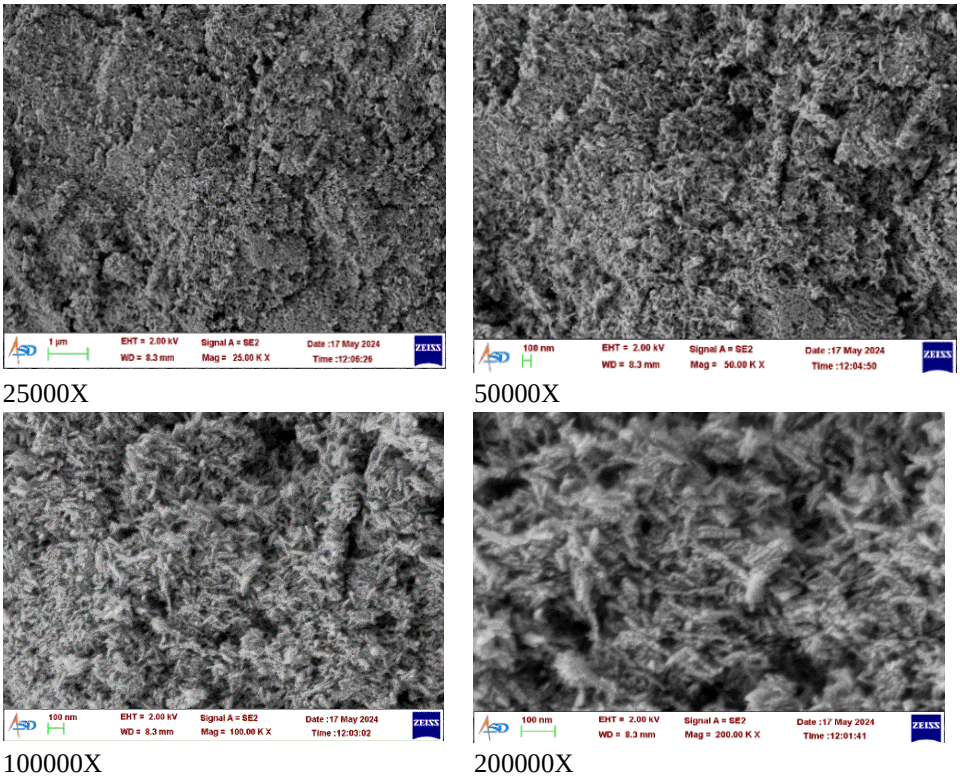

Fig. 12: SEM photo plates of IO-3 with different magnifications

c) Crystallography

1. XRD spectrum: Fig. 13 outlines the spectrum. Table-8 illustrates the corresponding peak positions including the derived particle size, Table-9 and 10 respectively depict the matching chemical composition from reference library, and crystal dimensions. The analysis indicates that these peaks align with the database entries for α-FeOOH

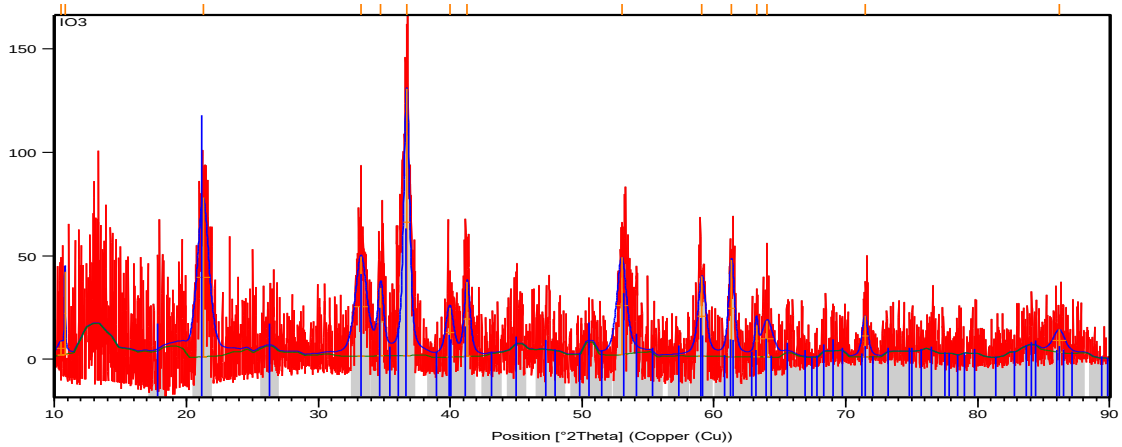

Fig. 13: XRD spectrum of IO-3

Table-8: Peak List of IO-3

Pos. [°2Th.]	Height [cts]	FWHM Left [°2Th.]	d-spacing [Å]	Rel. Int. [%]	size, nm
10.4726	6.52	0.6912	8.44037	5.06	11.7
10.7941	39.82	0.0864	8.18973	30.92	102.3
21.2758	76.84	1.0368	4.17278	59.65	7.9
33.2468	48.17	1.0368	2.69260	37.39	8.1

34.7427	32.70	0.5184	2.58002	25.38	16.3
36.7106	128.81	0.5184	2.44610	100.00	16.4
39.9698	23.88	0.6912	2.25383	18.54	12.4
41.2986	35.97	0.5184	2.18434	27.92	16.6
53.0147	47.08	0.8640	1.72592	36.55	10.4
59.1048	38.53	0.6912	1.56178	29.91	13.4
61.3500	46.83	0.5184	1.50989	36.35	18.1
63.2289	15.41	0.2592	1.46947	11.96	37.2
64.0493	17.60	1.0368	1.45262	13.66	9.1
71.4683	19.78	0.5184	1.31895	15.36	19.2
86.1910	11.08	1.0368	1.12746	8.60	10.6

Table-9: Composition of IO-3 as derived from XRD

Reference Code	Compound Name	Chemical Formula	No. of formula units per unit cell	Calculated density
01-081-0462	Goethite	FeO(OH)	4	4.24 g/cm^3

Table-10: Crystal dimensions of the components of IO-3 as derived from XRD

Compound Name	Crystal System	Space group	a, Å	b, Å	c, Å	α	β	γ
Goethite	Orthorhombic	Pbnm	4.6188	9.9528	3.0236	90^0	90^0	120^0

2. EDS Spectrum: The EDS spectrum is shown in Fig. 14. similar to IO-2, the sample is goethite with possible impurities and occluded moisture affecting the exact percentages.

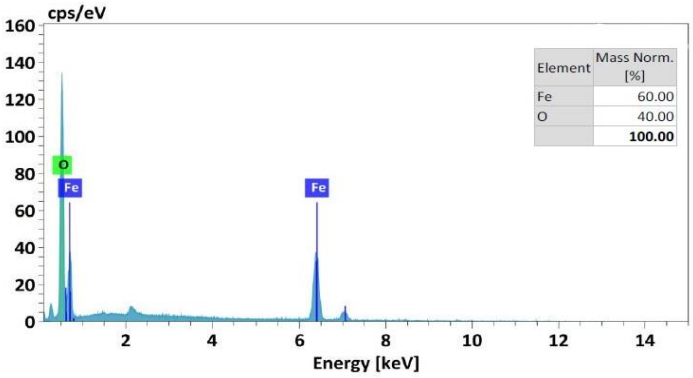

Fig. 14: EDS spectrum of IO-3

3. FTIR Spectrum: Fig. 15 showcases the FTIR spectrum of IO-3. Here, 3126cm^{-1} and 612cm^{-1} are associated respectively with the O-H stretching and bending vibration of hydroxyl groups (OH), 1644cm^{-1} to the bending vibration of water molecules (HOH bending mode), 890cm^{-1} and 791cm^{-1} corresponds to the Fe-O stretching and bending vibration in iron oxides respectively, particularly characteristic of goethite. Hence, it is concluded that the sample IO-3 is goethite (α-FeOOH).

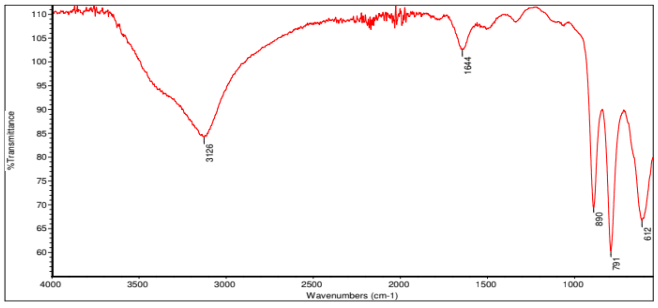

Fig. 15: FTIR Spectrum of IO-3

4. Raman Spectrum: Fig. 16 is the Raman spectrum signature. 219cm^{-1} is associated with the bending or deformation vibrations involving Fe-O bonds or bending modes of the hydroxyl (OH) groups in the goethite structure. 273 cm^{-1} is due to vibration modes related to the Fe-O-Fe linkages or stretching vibrations within the crystal lattice, corresponding to internal vibrations of the FeO_6 octahedra with in goethite. These octahedra are connected through edge-sharing, and this peak reflects vibrations involving these structural units. 383 cm^{-1} is related to the bending vibrations of the OH groups in goethite.

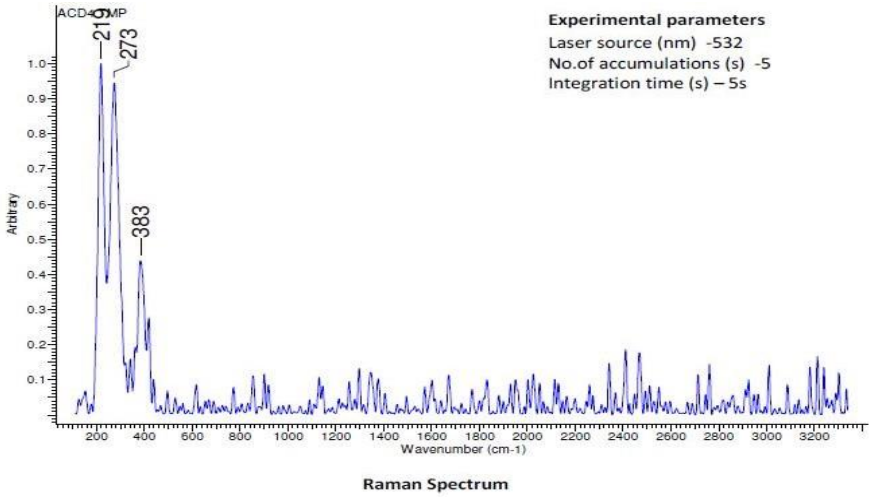

Fig. 16: Raman spectra of IO-3

5. Mossbauer Spectrum: The Mossbauer spectrum of IO-3 is shown in Fig. 17. The interpreted data is given in Table-11. From the table and the spectrum, it is concluded that the sample is similar to IO-2. However, the BHF value of <26.2> Tesla supports the presence of a hydrated iron oxide phase with the characteristics of hydrated goethite.

6.

Table-11: Mossbauer Spectrum Parameters of IO-3

Sample	Width (mm/s)	ISO (mm/s)	QUA (mm/s)	BHF (Tesla)	% Area
IO-3	0.45	-	-	<26.2>	100

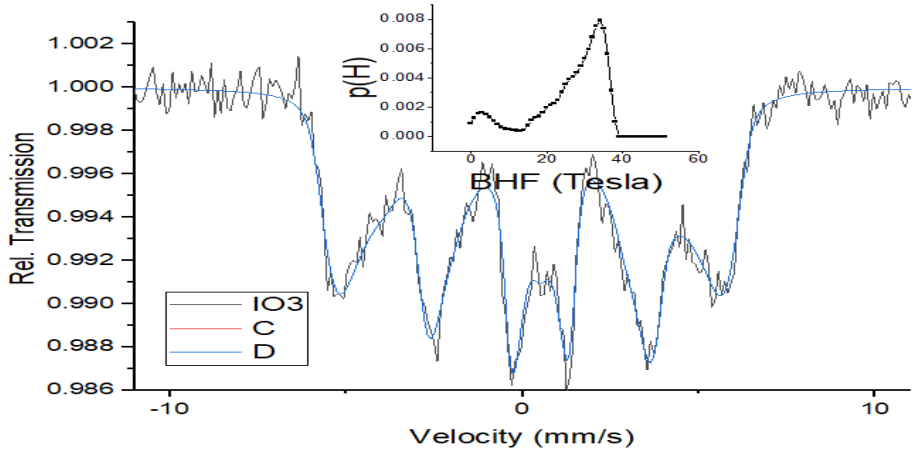

Fig. 17: Mossbauer Spectrum of IO-3

In summary, IO-3, which is prepared similar to IO-1 but is not exposed to higher temperature during process or during drying, since both took place at room temperature, yielded goethite (α-FeOOH) much similar to IO-2 with higher surface moisture. The particles are similar to IO-2, with large specific surface area, non-magnetic, rod-like/ fibrous/needle-like particles. The particles are highly randomly packed leading to a very high void fraction compared to IO-2, where the volatile matter (surface moisture) is entrapped in such a large quantity.

3.2. Propellant Characterisation Results and discussion

Solid rocket composite Propellant is prepared which is referred as HTPB/AP/Al formula in the ratio of 14/68/18 by weight. In fact, HTPB means, it is the binder system that contain Hydroxyl Terminated Poly Butadiene polymer and 2,4 Toluene di isocyanate (TDI) as the hardener. AP, the ammonium perchlorate is the oxidiser and the aluminium is the fuel. The reaction between AP and Al produces required energy for rocket velocity and acceleration, and the catalyst decides the rate of combustion there by the power of the rocket.
During the preparation, the materials are all added leading to a slurry, which after transferring into the rocket chamber heated to cure and become hard. The cure reaction is between HTPB and TDI and is monitored by viscosity and its build up. The quality of mix is measured by 1) viscosity at the end of the mix after sample is received to the lab and 2) mechanical properties after curing. The effect of catalyst is to promote the combustion reaction while firing, which is commonly termed as burn rate, measured in kg/s or for a standard geometry and given density measured in mm/s. The following paragraphs compiled the characterisation of propellants made with different Iron Oxide samples and compared with the reference sample which is prepared without the catalyst.

A. Viscosity at the end of Mixing and Cure reaction Kinetics

Conventionally, all the propellant manufacturers follow viscosity at the end of mixing as one of the performance indicators of whether all ingredients are added, whether all the particles are wetted and whether the slurry is fit for casting into the rocket chamber. Hence when a new material is tried to be kept in the formulation, this parameter is the first measure. Table-12 provides viscosity measured every 30 minutes for 3 hrs and Fig.18 is the corresponding plot.

The measurement uncertainty in the Brookfield viscometer, which was used for measuring the viscosity at constant rpm (hence constant shear rate) is about 10 Poise, half of least count.
From the table it is understood that viscosity of all the samples at 30 min (called End-of-mixing viscosity) are equal inferring that the particle sizes of all ingredients, mutual ratios of ingredients are within the experimental error. That is, the ferric oxide did not affect the End-of-mixing viscosity. The rate of change of viscosity is one measure of cure kinetics. Assuming, first order kinetics, the rate constant is proportional to viscosity rate constant. The rate constant is influenced by the moisture present, that can react with TDI, thereby reducing the availability of TDI molecules. Hence the data is regressed using exponential fit as shown in Fig.18 and the corresponding slope (rate constant) and intercept (estimated at zero time or immediate end of mixing, before taking the sample for testing). It is inferred that the change in catalyst did not affect cure kinetics although there is an indication that Propellant with IO-3 is resulted in lower rate of viscosity, which probably can be explained by the fact that IO-3 contain high % of surface moisture which interferes in HTPB-TDI reaction. For the sake of brevity and since the propellant making is not the main theme of the research work, further discussion is withdrawn.

Table-12: Propellant Viscosity for various samples with Iron Oxide

Time minutes	Viscosity (Poise)					
	Reference Sample	IO-1	IO-2	IO-3	IO-6	IO-8
30	8260	8840	8360	7860	8740	8480
60	7680	8580	7780	7640	8140	8060
90	8540	9460	8640	8340	8780	8840
120	8880	10020	8980	8540	9300	9240
150	9240	10220	9450	9020	10020	10040
180	9860	10680	10040	9340	10580	10240
Slope	12.40	13.98	13.10	11.18	14.63	14.42
Intercept	7441	8165	7500	7283	7724	7636

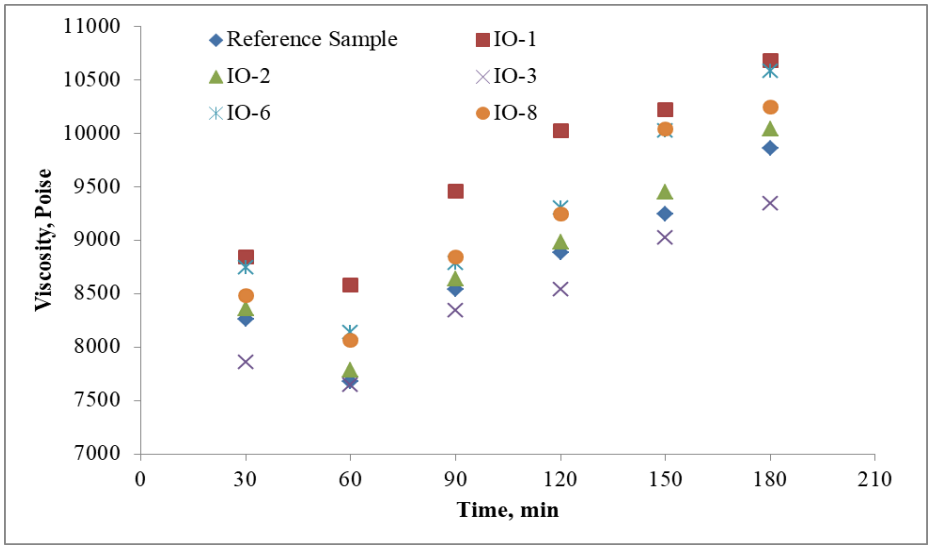

Fig. 18: Propellant Viscosity for various samples with Iron Oxide

B. Uniaxial Mechanical Properties and density

After curing, the propellant becomes sufficiently hard and rubbery, gaining mechanical strength. When a load (applied stress) is exerted on the propellant, such as in the direction of gravity, the rubbery material elongates (resultant strain) along the direction of the applied force. The ratio of stress to strain, known as Young's Modulus (or engineering strain), holds as long as the stress and strain remain within the Hookean (elastic) zone. The strength, elongation, and modulus are determined by the material composition—specifically, the relative proportions of ingredients—as well as factors affecting cure kinetics, such as surface moisture, and factors influencing test conditions and potential instrument errors. The tensile strength, modulus, and hardness of the IO-2 and IO-3 propellant samples are significantly lower. This reduction can be attributed to relatively high surface moisture, which consumed a portion of the TDI. Additionally, the needle-like structure of the particles creates voids that cannot be accessed by the HTPB-TDI network, leading to a reduced surface area for solid-polymer network bonding.

Table-13: Propellant Mechanical Properties for various samples with Iron Oxide

Mechanical Properties	Reference Sample	IO-2	IO-3
Tensile Strength (ksc)	9.0	5.4	4.0
Elongation at Break (%)	39	48	51
Modulus (ksc)	53	24	15
Hardness (Shore 'A')	71	55	53
Density (g/cc)	1.767	1.769	1.767

C. Propellant burn rate

Propellant burn rate is the actual measure of the function of the catalyst in the propellant. Iron oxide catalyst is expected to enhance the burn rate of the propellant by 1) decreasing the activation energy and combustion temperature of the selective reaction mechanisms of the propellant combustion 2) change the course of reactions in combustion. We tried to establish whether the developed experimental Iron oxide is capable of increasing the burn rate and whether it is due to the crystal structure.

Two different methods, well established industrially, are used to estimate the burn rate of propellant strands by burning at a predetermined pressure. One method captures the acoustic emission signature released during the

combustion, called AEBR and the other method captures the ultrasonic signature released during the combustion, termed UBR. The AEBR data is generated atone single pressure of 40ksc for different samples. On the other hand, UBR is carried out elaborately, specimens are burned at different pressures during different phases of specimen burning. This leads to deriving the pressure index value by fitting into veille's burn rate law. AEBR data at 40ksc is outlined in Table-14, whereas the corresponding UBR data is provided in Table-15.

Table-14: Propellant Burn rate measured using acoustic emission signature

Burn rate (AEBR)	Reference Sample	IO-2	IO-3
AEBR @ 40ksc (mm/s)	5.34	7.52	8.32

Table-15: UBR, at different pressures (~30-60 ksc) and pressure index

UBR Sample	Specimen number	Specimen burning rate (mm/s) at 40 ksc	Average, (Std. dev.)	Burning rate index (n-value)
Reference Sample	B1	6.011	6.039 (0.037)	0.297
	B2	6.061		
	B3	5.990		
	B4	6.052		
	B5	6.080		
	B2	7.981		
	B3	7.964		
	B4	7.905		
	B5	7.936		
IO-2	B1	8.196	8.168 (0.058)	0.396
	B2	8.235		
	B3	8.193		
	B4	8.121		
	B5	8.096		
IO-3	B1	8.817	8.802 (0.081)	0.448
	B2	8.741		
	B3	8.817		
	B4	8.715		
	B5	8.922		

4. Conclusions

The study confirmed that goethite structures, with their superior catalytic performance in propellants, are a promising alternative to conventional iron oxide catalysts, offering advantages such as higher burn rates, increased surface area, and phase transformation benefits. These results are ground breaking, with implications for the future of rocket propulsion in India and beyond.

5. Acknowledgements

The authors sincerely acknowledge SDSC-SHAR, ISRO for their invaluable support in conducting propellant trials and providing facilities for detailed characterization. This work would not have been possible without their technical expertise, resources, and guidance. The authors deeply appreciate their contribution to advancing the research objectives.

References

[1] S. Venkatachalam, G. Santhosh, K.N. Ninan, "High Energy Oxidizers for Advanced Solid Propellants and Explosives" Advances in Solid Propellant Technology, Ist International HEMSI Workshop, Ranchi, India, 2002, 87-106.

[2] Sarner S.F, Propellant Chemistry, Reinholt, New York, 1966.

[3] Victor Linder, Explosives and Propellants – Encyclopedia of Chemical Technology, Kirk Oathmer (ed.), 3rd ed., John Wiley, New York, 1980, 9, 620-671.

[4] Kishore, K & Sunitha, M.R. Effect of transition metal oxides on decomposition and deflagration of solid propellant system: a survey. AIAA. J, 1979, 17(10), 1118-25.

[5] David, I. and Welch, J. E. (1956) The oxidation of magnetite and related spinels. Constitution of gamma ferric oxide. Trans. Faraday SOC. 52: 1642.